A NOVEL VORTEX COMBUSTION DEVICE
Experiments and Numerical Simulations with Emphasis on the Combustion Process and NO_x Emissions

by

Abay DOSTIYAROV[a], Jordan HRISTOV[b], Dias UMYSHEV[c*], Ayaulym YAMANBEKOVA[a], and Zhanat OZHIKENOVA[a]

[a] G. Daukeev Almaty University of Power Engineering and Telecommunications, Almaty, Kazakhstan
[b] University of Chemical Technology and Metallurgy, Sofia, Bulgaria
[c] Satbayev University, Almaty, Kazakhstan

Original scientific paper
https://doi.org/10.2298/TSCI210920011D

Experimental and numerical studies of combustion process in a vortex flow device have been developed. The modelling part of the study has been performed by means of ANSYS Fluent package. Fuel droplet trajectories and the flow pattern on their motions have been modeled by the function "injection". The combustion process utilized the k-ε turbulence model. A special trend on the effect of the vortex generator blade orientation on the gross process has been developed. It has been established that optimal process performance (high air excess ratio and low NO_x emissions) could be attained with an angle of the vortex generator blade orientation, especially with respect to the minimization of NO_x emissions.

Key words: *combustion device, NO_x, vortex flow, turbulence model*

Introduction

This Premixed combustion of fuels in various devices is a process allowing mitigation of toxic components emissions [1-6]. In this context, premixed combustion of bamboo particles revealed that the excess of combustible yield increase in the combustion rate since it directly affects the time scale of the chemical reaction and the turbulent flow through the Karlovitz number [2] *i.e.* inverse to the Damkohler number. An important part of the combustion process performance is the gross hydrodynamic flow resistance due to the use of vortex generators and bluff bodies [7, 8]. The reduction of NO_x emissions may be reduced as a result of optimal flow patterns created by suitable vortex generations, compositions of bluff bodies and leaning initial fuel-air composition [9, 10]. In this context, the oxygen excess in a vortex chamber up to 20% allows reduction of NO_x emissions down 23,8% [11, 12]. Numerical studies on NO_x emissions in a vortex revealed the increase in the mixing efficiency reduces significantly the formation and emissions of toxic combustion byproducts [11, 13]. For example, in [12], the influence of the initial air swirl was investigated, which led to a decrease in the formation of NO_x, as well as to an increase in the CO concentration. In [14], the influence of fuel supply on the EV burner, which supplies fuel with swirling, was studied. Studies have shown that the formation processes

* Corresponding author, e-mails: d.umyshev@satbayev.university; umishev_d@mail.ru

are affected by the supply of secondary air, in particular, by the residence time of gases in the combustion zone and the mixing of fuel with air.

The importance of both the combustion efficiency and the environmental impact forms special demand on the combustion devices constructions [15, 16]. Following this line, the present work addresses experimental and numerical studies of new combustion device with the premised fuel-oxidant flow.

In Kazakhstan, there are a large number of agricultural enterprises that use heat generators to dry various types of plants, so they most often use portable heat generators on liquid fuel. However, all the growing requirements for environmental pollution in Kazakhstan [17] require the reduction of harmful emissions with an increasing level of drying quality.

Another problem is the pollution of the environment by boilers when using solid fuels in urban areas. To solve this problem, the country faces the task of switching to liquid and gaseous fuels [18].

Based on the analysis, the authors concluded that in the conditions of Kazakhstan, for heat generators and boiler units, it is necessary to develop new types of burners with a reduced formation of toxic substances, in particular NO_x. Based on the literature analysis, the authors concluded that the most suitable methods are preliminary fuel preparation and staged fuel supply to the combustion zone. This article presents the results of experimental and numerical studies of a burner with preliminary fuel mixing and staged air supply.

Experimental set-up

The combustion device was studied by a set-up shown schematically in fig. 1. The supply by a fan allowed the air-flow to be varied in the wide range. The velocity profile is stabilized by the bundle of parallel tubes. The exhaust gases were analyzed by a gas analyzer permitting simultaneous measurements of concentrations and temperatures.

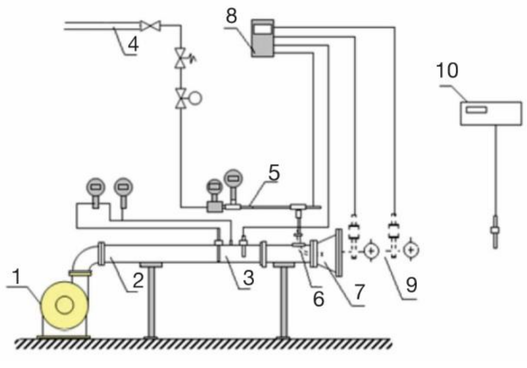

Figure 1. Experimental set-up;
1 – fan, 2 – stabilizing flow tube bundle, 3 – measurement point at the flow entrance, 4 – gas flow supply, 5 –measurement point for fuel supply, 6 – fuel supply tube, 7 – front diffusor with the combustion chamber, 8 –multichannel data acquiring system, 9 – measurement point behind the diffusor, 10 – gas analyzer

The experimental set-up consists of an atmospheric fan – 1 for air supply with a flow rate of 500-3000 m^3/h. The fan was controlled by a speed control system (not shown in the diagram). To stabilize the flow, – 2 with a length of 500 mm was used. To account for the fuel consumption, a flow meter – 5 was used. Fuel was supplied through a fuel supply pipe – 6. The combustion process was behind the front diffuser – 7.

Dimensions of combustion chamber are given in tab. 1.

Combustion device

The general view of the combustion device shown in fig. 2 reveals that it consists of an entrance blade vortex generator, an existing vortex generator, a device for a secondary air supply, and a nozzle for the liquid fuel (kerosene) supply (located at the symmetry axis of the combustion device). Thermophysical parameters of kerosene are presented in tab. 2. In this experiment, we studied combustion with a large excess of air, because these burners must be used in heat generators where it is necessary to produce large quantities of hot gases for drying. This type of combustion reduces combustion efficiency, but heats up a large amount of air.

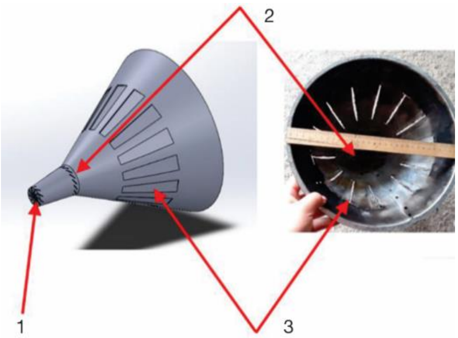

Figure 2. General view of the combustion device; *1 – entrance vortex generator, 2 – exist vortex generator, 3 – slits for secondary air supply*

The ignition was carried out by an electrical spark igniter, located just after the profile. The temperature of the exhaust gases was measured by Cr/Al thermocouples (0.5 mm in diameter) positioned symmetrically with respect to the combustion chamber symmetry axis. The exhaust gases contents were monitored and measured (with a maximal error of 5 %) by a portable gas analyzer (Testo 350-XL).

Table 1. Dimension of combustion chamber

Property	Unit	Value
Length	mm	310
Inlet diameter	mm	35
Outlet diameter	mm	295
Length of the vortex device	mm	80

Table 2. Thermophysical parameters of kerosene

Property	Unit	Value
Density at 20 °C	[kgm^{-3}]	778
Lower heating value, Q^w_l	[kJkg^{-1}]	42900
Mass fraction of sulfur	[%]	0.25<
Mass fraction of hydrogen sulfide	[%]	0

The devices used in the experiments and their error margins are presented in tab. 3.

Table 3. The devices used in the experiments and their error margins

Device	Measurements	Error margin
Thermocouple TXA (Cr/Al)	Exhaust gas temperature	Measurement error up to 300 °C: 0.1 °C
		above 300 °C: 1 °C.
Thermocouple sensor devices	Thermo EMF from thermocouple	In the range from -40 to +375°C: ± 1.5°C
		In the range over plus 375 to plus 1100°C: ± 0.004*measured temperature
Gas analyzer Testo350-XL	Exhaust gas temperature	5% over the entire measuring range
	Exhaust gas composition (NO_x and O_2)	
Vane anemometer Testo 416	Air velocity	±0.2 m/s+1.5% of measured values
Differential pressure gauge KM-11	Outlet pressure	±2.5% for whole range of measures

The Testo 350-XL gas analyzer measures the concentration of NO_x in ppm. For the translation based on the concentration of nitrogen oxides, the formula was used:

$$\mathrm{NO}_{x\,\mathrm{at}\,\mathrm{O}_2} = \frac{\mathrm{NO}_x\,[\mathrm{ppm}]}{21-\mathrm{O}_2} \tag{1}$$

Concentration of O_2 was measured by gas analyzer.

Conversion in [$\mathrm{mgm^{-3}}$] was carried out according to the formula:

$$\mathrm{NO}_{\mathrm{mg/m^3}} = \frac{\mathrm{NO}_{x\,\mathrm{at}\,\mathrm{O}_2}30}{22.4} \tag{2}$$

To calculate the friction coefficient, the velocities and pressures at the outlet from the experimental set-up were measured. The velocity was measured with an anemometer, pressure with a manometer. The technical specifications of the devices are presented in tab. 2. The friction coefficient was calculated according to the formula:

$$\xi = \frac{\Delta l}{\rho\omega^2} \tag{3}$$

Air excess ratio was calculated as following:

$$\alpha = \frac{\left(\dfrac{m_{\mathrm{air}}}{m_{\mathrm{fuel}}}\right)_{\mathrm{stoich.}}}{\left(\dfrac{m_{\mathrm{air}}}{m_{\mathrm{fuel}}}\right)_{\mathrm{act.}}} = \frac{1}{\varphi} \tag{4}$$

Combustion efficiency was calculated by following formula:

$$\eta_c = \frac{(1+L_0\alpha)(C_{p,\mathrm{g}}T_{\mathrm{exp.}} - C_{p,\mathrm{g}}T_0) - L_0\alpha(C_{p,\mathrm{air}}T_{\mathrm{exp.}} - C_{p,\mathrm{air}}T_0) - (C_{p,\mathrm{g}}T_{\mathrm{exp.}} - C_{p,\mathrm{g}}T_0)}{Q_1^w} \tag{5}$$

Swirl number was calculated by following formula:

$$SW = \frac{G_\beta}{G_x R} = \frac{2}{3}\left[\frac{1-\left(\dfrac{R_h}{R}\right)^3}{1-\left(\dfrac{R_h}{R}\right)^2}\right]\tan\beta_2 \tag{6}$$

The average Sauter diameter, D_s, which is the diameter of a droplet, for which the ratio of volume to surface area is equal to this ratio for all droplets. The diameter was calculated using the formula [19]:

$$D_\mathrm{s} = \frac{0.19}{\omega}\left(\frac{\sigma_{\mathrm{fuel}}}{\sigma_{\mathrm{fuel}}\sigma_{\mathrm{air}}}\right)^{0.35}\left(1+\frac{m_{\mathrm{fuel}}}{m_{\mathrm{air}}}\right)^{0.25} + 0.127\left(\frac{\mu^2 d_0}{\sigma_{\mathrm{fuel}}\rho_{\mathrm{fuel}}}\right)^{0.5}\left(1+\frac{m_{\mathrm{fuel}}}{m_{\mathrm{air}}}\right) \tag{7}$$

Numerical modeling

The numerical simulation of the combustion device work was carried out with the geometric model shown in fig. 3 and related to kerosene combustion. Kerosene was chosen as a fuel since this type of fuel was used in experimental studies. The model of the combustion device consists of: entrance vortex generator with variable blade angle orientation, exit vortex generator with fixed blades. The fuel was supplied at the symmetry axis of the combustion chamber.

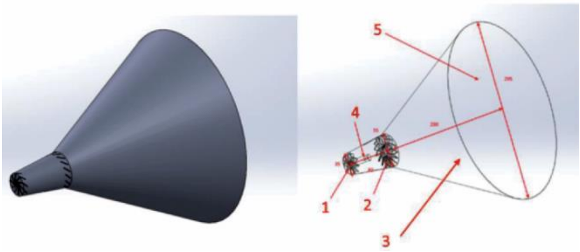

Figure 3. Model for numerical studies; *1 – entrance vortex generator, 2 – exist vortex generator, 3 – slits for secondary air supply (not shown), 4 – fuel inlet, 5 - outlet of the model*

Mathematical model

Previous studies of combustion processes have shown that the turbulence model has a sufficient level of accuracy [15, 16], which determined the choice of this model. The injection model was used to model liquid fuel injection. Model P-1 was chosen for the simulation of radiation since it consumes less computational resources. For the combustion process, a one-stage reaction mechanism is adopted. Taking into account that the reaction rate of the vortex dissipation model is controlled by turbulent mixing, the vortex dissipation model is used in this work. The combustion in the combustion chamber is non-premixed combustion, and the liquid fuel and air enter the combustion zone, respectively. Heat transfer is mainly dependent on radiation and convection. Boundary conditions are presented in tab. 4.

Table 4. Boundary conditions

Measure	Unit	Value
Air-flow	m^3h^{-1}	500-3000
Fuel-flow	kgh^{-1}	1
Fuel temperature	K	288
Air temperature	K	288

The governing equation in accordance with the k-ε turbulence models [6] are:

– Continuity equation:

$$\frac{\partial p}{\partial t}+\frac{\partial (pu_i)}{\partial x_i}=0 \tag{8}$$

– Momentum equation:

$$\frac{\partial (\rho u_i u_j)}{\partial x_i}+\frac{\partial (p)}{\partial x_i}+\frac{\partial \tau_{ij}}{\partial x_j} \tag{9}$$

– Energy equation:

$$\frac{\partial(\rho u_i h)}{\partial x_i} + \frac{\partial}{\partial x_i}\left(\lambda_{\mathrm{f}} \frac{\Delta T}{\partial x_i}\right) + \sum_j \left[\frac{\partial}{x_i}\left(D_{j,m}\rho h_j \frac{\partial Y_j}{\partial x_i}\right)\right] + q \tag{10}$$

– State of ideal gas:

$$p = \rho \mathrm{R_g} T \sum_{s=1}^{Ng} \frac{Y_\mathrm{s}}{M_\mathrm{s}} \tag{11}$$

Works on numerical modeling show that the final results are largely affected by the heat transfer process between solids and gases. Therefore, given that steel was used in the experimental bench, the thermal conductivity of the bluff body and walls was 42.5 W/mK. Energy equation for a solid:

$$\frac{\mathrm{d}(k_\mathrm{s} \mathrm{d}T)}{\mathrm{d}x^2} + \frac{\mathrm{d}(k_\mathrm{s} \mathrm{d}T)}{\mathrm{d}y^2} = 0 \tag{12}$$

Grid independence study

To confirm the numerical simulation, we compared the experimental results with the calculation results. The dimensions of the combustion chamber model are the same as in experimental studies and presented in tab. 1. The average gas temperatures at the outlet of the combustion and simulation chamber are shown in tab. 5. The temperatures were taken as average values over the cross-section at the exit from the simulation zone and the experimental set-up. A temperature comparison shows good convergence. To save the calculation time, we used grids with sizes of 2 mm, 3 mm, and 6 mm (the relevant information is summarized in tab. 4. Additional information about the physical situations simulated is presented in tab. 5.

Table 5. Grid independence study results

Grid	Element numbers	Outlet temperature (simulation) $T_{\mathrm{sim.}}$ [K]	Outlet temperature (experiment) T_{exp} [K]	Difference [%] 100 $(T_{\mathrm{exp}} - T_{\mathrm{sim}})/T_{\mathrm{exp}}$
2 mm	1531546	338	324	4%
3 mm	1111283	352		8.6%
6 mm	874351	365		12%

To confirm the obtained data, we compared the obtained temperatures at the outlet of the experimental set-up and the results of numerical simulation for $\beta_2 = 60°$. The comparison results are presented in tab. 6. The difference in the data obtained does not exceed 12%. Additionally, a comparison of the concentration of nitrogen oxides was carried out. For the calculations, a 3 mm grid size of the mesh was chosen, since it has a relatively low error and takes a relatively short time for calculations.

The air-droplet flow was simulated by the function injection. The fuel flow rate was established at 0.001 kg/s and the droplet diameter was established at about 1 mm [19].

Table 6. Initial model parameters

Angle of the blade in the exist vortex generator, β_2	Air-flow rate [kgs^{-1}]	Initial temperature of the oxidant (air) fuel mixture [K]	Amount of tetradic elements in the modelling area	Swirl number
20º	20	400	200000	0.67
30º				1.06
60º				3.23

The combustion problem solution used the model of partial premixing since this approach is highly efficient when liquid droplet combustion is simulated; taking into account the fuel vaporization and drop radius change in time [6, 7].

Results

The friction factor coefficients are shown in fig. 4 as a function of the vortex generator blade orientation and the ratio r_1/r_2 of the entrance to exit diameter. These plots indicate that a minimum in flow resistance can be attained at the angle of blade orientation of 60°. Further increase in the angle inclination yields a decrease in the area of the flow passage and an increase in the drag resistance. At the same time the increase in the entrance flow area (increase in) reasonable reduces the drag resistance.

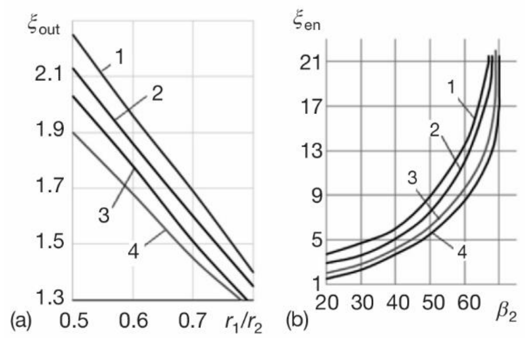

Figure 4. Friction coefficients of the vortex generators for various angles of the (a) blade orientations and (b) entrance to exist radius ratio r_1/r_2; (a) entrance vortex generator. Blade angle: 1 – β_2^0 = 30°, 2 – β_2^0 = 40°, 3 – β_2^0 = 50°, 4 – β_2^0 = 60°, (b) exit flow generator. Radius ratio: 1 – r_1/r_2 = 0.32, 2 – r_1/r_2 = 0.51, 3 – r_1/r_2 = 0.635, 4 – r_1/r_2 = 0.725

The combustion efficiency as a function of the air excess is shown in fig. 5. It indicates that the maximum in the combustion process efficiency can be attained at α = 4.5. At minimal air-flow excess the completeness of the combustion reduces while the increase in the air-flow results in increased turbulence and swirling flow pattern, as well flow entrainment with elutriation of unburnt fuel droplets.

The concentration of NO_x as a function of the airflow excess shown in fig. 6 reveals that the increase in the air-flow yields reduction in NO_x concentration. At the minimum air-flow excess, the NO_x concentration is 50 mg/m^3. According to BAT [20] Table 10.14, the average annual emissions of new power plants with a capacity below 100 MW should be in the range of 75-200 mg/m^3. Additionally, the results were compared with [21], the presented burner allows to reduce the concentration of NO_x up to 20% compared to the heat generators which are currently used. When installing the developed burner in the amount of three pieces into the boiler, the average annual emissions will not exceed 150 mg/m^3. Further increase in the air-flow yields more efficient mixing of the fuel which finally results in minimization of local high temperature zones where mainly NO_x are generated. Concentrations of NO_x presented in fig. 6 were calculated using eq. (2) and for reference concentration of 15% O_2. The NO_x concentrations shown in fig. 6 were calculated using eq. (2) and for 15% O_2 as a reference level.

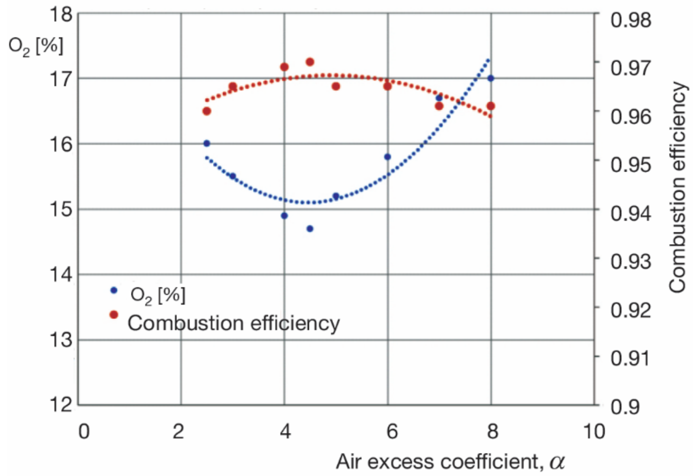

Figure 5. Coefficient of the combustion efficiency (completeness) and O_2 concentrations [%] in the air-driven nozzle as function of the total air flow excess

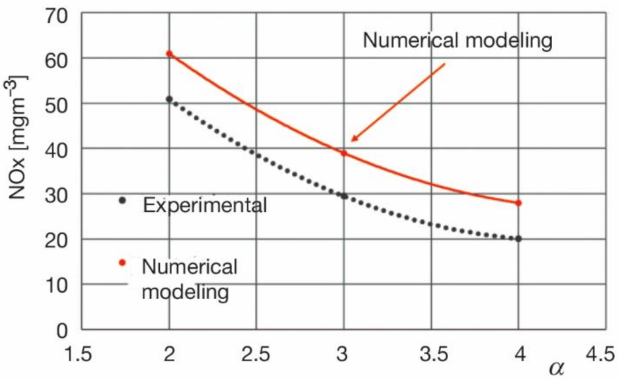

Figure 6. Exist concentration of NO_x as a function of the air flow excess

The concentration of NO_x as a function of the blade angle orientation in the entrance vortex generator are shown in fig. 7. The experiments reveal that the increase in the blade angle yield increased circulation zone as therefore the number of circulating gases, that is the residence time of the fuel in the high temperature zone increases, hence, the NO_x emission is greater than when $\beta_1 = 40°$. It is worthy to stress the attention on the fact that at small angles the is flow instability (flow detachment from the diffusor wall) and the amount of the gas circulating in this section is greater than in the central chamber zone that also increasing the fuel residence time and consequently high level of NO_x emissions. The maximal NO_x level in the entire range of the air-flow excess variations was attained at a blade angle of 40°. The NO_x concentrations shown in fig. 7 were calculated using eq. (2) and for 15% O_2 as a reference level.

In a situation, without an entrance vortex generator, the maxim of the NO_x concentrations can be attained when $\beta_2 = 60°$ and air-flow excess coefficient as shown in fig. 8. The reduction in the air-flow excess results in a stable torch only when $\beta_2 = 60°$. In other regimes when the maximal NO_x concentrations correspond to β_2 = 20° and reduction in the air-flow excess the NO_x level reduces. The increase in the vortex blade angle results in an enlarged circulation zone and increase fuel that finally increases the level of NO_x. The NO_x concentrations shown in fig. 8 were calculated using eq. (2) and for 15% O_2 as a reference level.

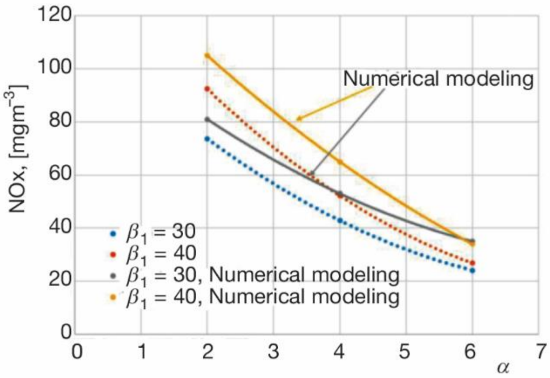

Figure 7. Effect of the blade orientation in the entrance vortex generator on the level of NO_x formation

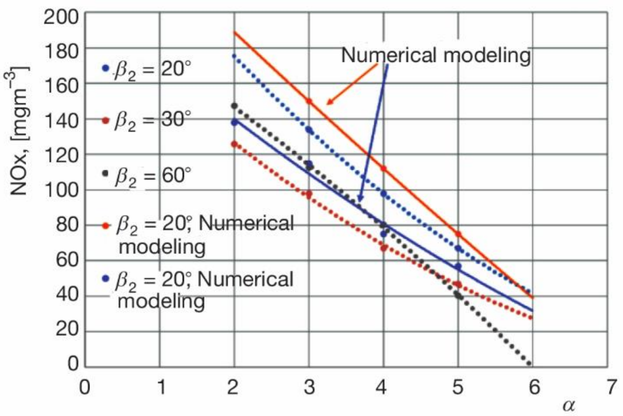

Figure 8. The NO_x level at the exit as a function of the air flow excess in case without entrance flow generator

The temperature profiles in fig. 9 show the effects of the process conditions. The almost acceptable flow distribution map corresponds to the case with the angle of the blade about 30°. Reduction in the blade angle yields increased vortices generation. With maximal blade angle, the flame has an almost symmetrical structure with a *neck* corresponding to the high temperature zone. Geometrically this zone corresponds to the zone where the fuel droplets vaporization takes place. The increase in flow swirling yields increased flow turbulence and the flame shape become asymmetrical. The latter can be attributed to increased turbulence scale and turbulence pulsations that finally yield combustion in asymmetrically formed flame. With 60° of blade angle, there is the visible flame there is no combustion process due to the high centrifugal forces direct the droplets towards the wall and due to insufficient heat transfer to the drops assuring their vaporization the combustion process conditions cannot be attained.

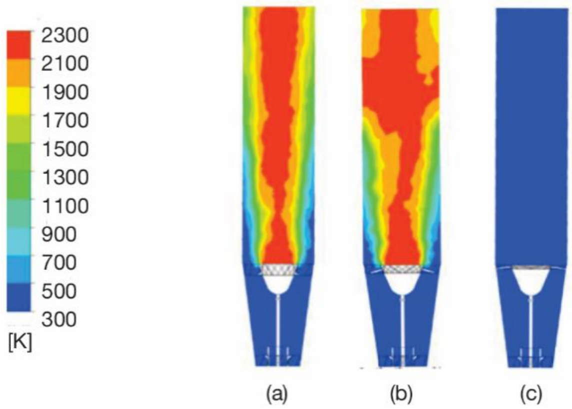

Figure 9. Temperature profiles; (a) 20°, (b) 30°, and (c) 60°

The flow maps in fig. 10 show clearly the blade angle orientation effects. It is obvious that at 20° there is a well-developed recirculation zone after the cone assuring flow stability. Here, it should be stressed the attention on the results in [8] revealing that the increase in the flame turbulence is a result of the so-called *auto turbulization* effect. This is confirmed by fact that the increase in blade angle up to 60° is followed by an increase in the flame speed and the growth zone approaches the torch base. The increase in blade angle up to 60° is not followed by sharp jumps in the flow field and the maxima are close to the near-wall zone as a consequence of increased centrifugal forces effects.

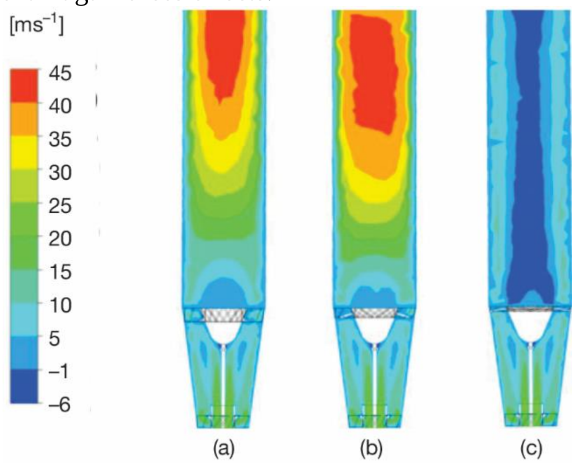

Figure 10. Flow map (velocity profiles) at various blade angles; (a) 20°, (b) 30°, and (c) 60°

Figure 11 shows the trajectories of particles at different angles β_2. As can be seen from the figures, at an angle of $\beta_2 = 20°$, the flow swirls in a designated manner and their temperatures have a high temperature in ehe combustion zone. This is also shown by the experimental data, at $\beta_2 = 20°$, the NO_x concentrations have maximal values. An increase in the angle leads to an increase in the swirl number and the trajectory of the particles becomes more centrifugal, due to which the participation of particles in combustion is reduced and the temperatures decrease faster. This is noticeable in fig. 11(c).

At the maximum blade angle $\beta_2 = 60°$, the maximum swirl number is achieved, which leads to a decrease of the combustion efficiency and significant centrifugal flows, leading to a decrease of the exhaust gas temperatures.

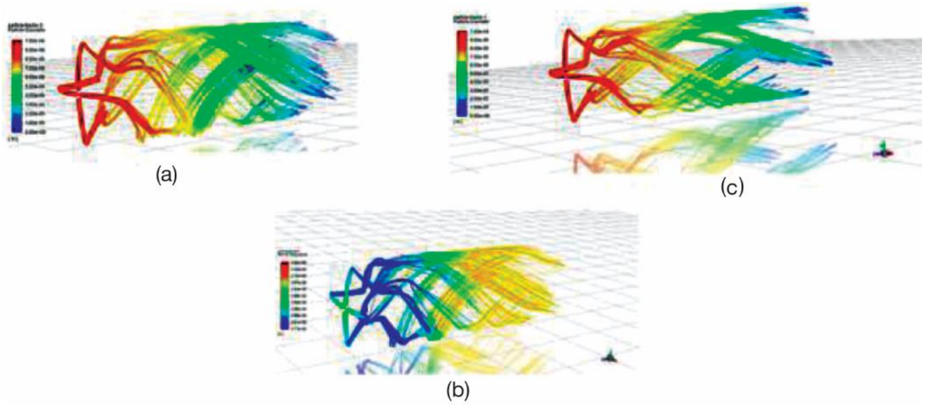

Figure 11. Particle trajectories simulated profiles and their temperatures; (a) 20°, (b) 30°, and (c) 60°

Conclusions

Experimental and numerical studies of the effect of the vortex generator have shown as follows.

- The efficient reduction in the NO_x emission in processes of lean premixed combustion of liquid fuels is possible to be controlled by the adequate flow swirling by inlet and exit vortex generators.
- With strong swirling of the flow, liquid droplets acquire centrifugal force and move along the wall of the burner, which negatively affects the completeness of combustion.
- Maximal combustion efficiency is achieved at $\alpha = 4.5$.
- Both the experimental results and the numerical simulations indicate that such minima in the NO_x concentrations can be attained when the blade angle is about 30° although in this case the flow drag increases. This angle is considered as optimal.
- The obtained experimental and numerical data make it possible to use the burner in the combustion chambers of the gas turbine units, and can also be used for the furnaces of low-power hot water and steam boilers. In case of use in heat generators, it is necessary to make calculations of standard sizes and installation. To use these burners on boilers, higher pressures and higher fuel consumption must be taken into account.

Nomenclature

$C_{p,\mathrm{g}}$ – heat capacity of exhaust gases, [kJkg^{-1}K^{-1}]
D' – dissipation coefficient, [–]
d_0 – fuel hole diameter, [mm]
G_x – axial flux of the axial momentum, [–]
G_β – axial flux of the tangential momentum, [–]
h – total enthalpy of gas mixture, [kJkg^{-1}]
h_j – enthalpy of j^{th} component, [kJkg^{-1}]
k_s – thermal conductivity of solid body, [Wm^{-1}k^{-1}]
L_0 – theoretically required amount of air, [m^{3}m^{-3}]
M_s – molecular mass, [gmol^{-1}]
Δl – manometer difference [m]
m_{air} – mass flow of air, [kgs^{-1}]
m_{fuel} – mass flow of fuel, [kgs^{-1}]
p – static pressure, [Pa]

q – heat of reaction [kJ]
Q_l^w – lower heating value of fuel, [kJkg^{-1}]
R – flow path radius, [mm]
$\mathrm{R_g}$ – universal gas constant
R_h – axial radious of the vortex generator, [mm]
T – temperature of reaction, [K]
Y_j – mass fraction of j^{th} component, [–]
T_{exp} – temperature on the outlet of the combustion chamber (experimental), [K]
T_{sim} – temperature on the outlet of the combustion chamber (simulation), [K]

Greek symbols

α – air excess coefficient, [–]
β_1 – angle of the entrance vortex generator, [°]
β_2 – angle of the outlet vortex generator, [°]
μ – orifice module, [–]
η_{c} – combustion efficiency, [–]
λ_{f} – thermal conductivity of fluid [Wm^{-1}K^{-1}]
ξ – friction factor coefficient, [–]
ρ – density, [kgm^{-3}]
ρ_{air} – air density [kgm^{-3}]
ρ_{fuel} – fuel density [kgm^{-3}]
σ_{fuel} – surface tension of fuel, [Nm^{-1}]
τ – turbulent stress, [–]
ω – exhaust gas velocity, [ms^{-1}]

References

[1] Amirreza, K., *et al.*, Mathematical Modeling of Multi-Region Premixed Combustion of Moist Bamboo Particles, *Renewable Energy*, *162* (2020), Dec., pp. 1618-1628
[2] Lee, J., Mueller, M., Closure Modeling for the Conditional Reynolds Stresses in Turbulent Premixed Combustion, *Proceedings of the Combustion Institute*, *38* (2021), 2, pp. 3031-3038
[3] Zhu, R., *et al.*, Combustion Instability Analysis on a Partially Premixed Swirl Combustor by Thermoacoustic Experiments and Modeling, *Energy*, *211* (2020), ID 118884
[4] Yang, T., *et al.*, Partially Premixed Combustion Optimization Using Double Injection Strategy in Transient Operation, *Applied Thermal Engineering*, *169* (2020), ID 114963
[5] Pollack, M., *et al.*, Evaluation of Quadrature-Based Moment Methods in Turbulent Premixed Combustion, *Proceedings of the Combustion Institute*, *38* (2020), 2, pp. 2877-2884
[6] El-Zoheiry, R. M., *et al.*, Combustion and Emission Characteristics of Jojoba Biodiesel-Jet A1 Mixtures Applying a Lean Premixed Pre-Vaporized Combustion Techniques: An Experimental Investigation, *Renewable Energy*, *162* (2020), Dec., pp. 2227-2245
[7] Vignat, G., *et al.*, An Experimental Study into the Effect of Injector Pressure Loss on Self-Sustained Combustion Instabilities in a Swirled Spray Burner, *Proceedings of the Combustion Institute*, *37* (2019), 4, pp. 5205-5213
[8] Chen, Z., *et al.*, Anthracite Combustion Characteristics and NOx Formation of a 300 MWe Down-Fired Boiler with Swirl Burners at Different Loads after the Implementation of a New Combustion System, *Applied Energy*, *189* (2017), Mar., pp. 133-141
[9] Li, Z., *et al.*, Effects of Particle Concentration Variation in the Primary Air Duct on Combustion Characteristics and NOx Emissions in a 0.5-MW Test Facility with Pulverized Coal Swirl Burners, *Applied Thermal Engineering*, *73* (2014), 1, pp. 859-868
[10] Khanafer, K., Aithal, S. M., Fluid-Dynamic and NOx Computation in Swirl Burners, *International Journal of Heat and Mass Transfer*, *54* (2011), 23-24, pp. 5030-5038
[11] Zhou, H., *et al.*, Impact of OFA on Combustion and NOx Emissions of a Large-Scale Laboratory Furnace Fired by a Heavy-Oil Swirl Burner, *Applied Thermal Engineering*, *90* (2015), Nov., pp. 994-1006
[12] Jing, J., *et al.*, Influence of Primary Air Ratio on Flow and Combustion Characteristics and NOx Emissions of a New Swirl Coal Burner, *Energy*, *36* (2011), 2, pp. 1206-1213
[13] Li, S., *et al.*, Effect of Outer Secondary-Air Vane Angle on the Flow and Combustion Characteristics and NOx Formation of the Swirl Burner in a 300-MW Low-Volatile Coal-Fired Boiler with Deep Air Staging, *Journal of the Energy Institute*, *90* (2017), 2, pp. 239-256
[14] Cho, C. H., *et al.*, A Numerical Approach to Reduction of NOx Emission from Swirl Premix Burner in a Gas Turbine Combustor, *Applied Thermal Engineering*, *59* (2013), 2, pp. 454-463
[15] Umyshev, D. R., *et al.*, Experimental Investigation of Distance Between V-Gutters on Flame Stabilization and NOx Emissions, *Thermal Science*, *23* (2019), 5B, pp. 2971-2981
[16] Umyshev, D. R., *et al.*, Effects of Different Fuel Supply Types on Combustion Characteristics behind Group of V-Gutter Flame Holders: Experimental and Numerical Study, *Thermal Science*, *24* (2020), 1A, pp. 379-391

[17] ***, Environmental Code of the Republic of Kazakhstan (No 400-VI ЗРК), January 2, 2021, https://adilet.zan.kz/
[18] ***, Concept for the Development of the Fuel and Energy Complex of the Republic of Kazakhstan until 2030. Resolution of the Government of the Republic of Kazakhstan dated June 28, 2014 No. 724, https://adilet.zan.kz/
[19] Dostiyarov, A. M., Development of Fuel-Burning Arrangement with Microflame Burning and Method of Calculation, Ph. D. thesis, Kazakh National Energy Institue, Almaty, Kazakhstan, 2000
[20] ***, Best Available Techniques (BAT) Reference Document for Large Combustion Plants. Industrial Emissions Directive 2010/75/EU Integrated Pollution Prevention and control, EU, 2017. http://www.publications.jrc.ec.europa.eu
[21] Ezhov, V. S., *et al*., Hazardous Emissions of Heat Power Plants into the Atmosphere and Method of Purification of Smoke Gases of Autonomous Heat Supply Heat Generators, *Proceedings*, Youth and science: a step to success Conf., Kursk, Russia, 2019, Vol. 5, pp. 145-149

Paper submitted: September 20, 2021
Paper revised: January 10, 2022
Paper accepted: January 13, 2022